Influence of the Anticyclonic Anomaly in the Subtropical Jet over the Western Tibetan Plateau on the Intraseasonal Variability of the Summer Asian Monsoon in Early Summer

TAKESHI WATANABE

Graduate School of Environmental Science, Hokkaido University, Sapporo, Japan

KOJI YAMAZAKI

Faculty of Environmental Earth Science, Hokkaido University, Sapporo, Japan

(Manuscript received 14 January 2011, in final form 22 August 2011)

ABSTRACT

The upper-level troposphere over the western Tibetan Plateau, where the subtropical jet is located in summer, is a region of marked intraseasonal variability in geopotential height (GPH). This study investigates the influence of an anomaly in this region on the summer Asian monsoon. To this end, the GPH index is defined as the daily geopotential height anomaly at 200 hPa over the region based on 40-yr European Centre for Medium-Range Weather Forecasts Re-Analysis (ERA-40) data. Composites with respect to strongly positive values of the GPH index are analyzed.

The results indicate that the temporary anomaly in the subtropical jet influences the monsoon over South Asia, Southeast Asia, and probably also over East Asia, because of two main processes: the eastward propagation of quasi-stationary Rossby wave anomalies at upper and lower levels along the subtropical jet, and a belt of strong westerlies at 15°N (Arabian Sea–Bay of Bengal–the Philippines).

The two mechanisms that underlie the lower-level Rossby wave anomaly are discussed here for the first time, based on the Rossby ray-path theory, as follows: 1) anomalous descent generated by the upper-level anticyclonic anomaly over Afghanistan and the western Tibetan Plateau causes the development of a heat low over the Thar Desert and neighboring areas, and 2) an anomalous southwesterly appears over the Arabian Sea, accompanied by the heat low, and interacts with the Western Ghats, resulting in an anticyclonic anomaly over the Indian subcontinent. The anomaly then starts to propagate eastward along a Rossby waveguide.

1. Introduction

The Asian monsoon is one of the most important climate systems worldwide. Its variability has attracted great attention because of its major influence on not only those areas directly affected by the monsoon but also regions located farther afield, at various time scales ranging from diurnal to climatological (Rodwell and Hoskins 1996; Annamalai and Slingo 2001; Ding and Wang 2005; Duan and Wu 2005; Randel and Park 2006).

This study is concerned with the influence of high-latitude anomalies on the Asian monsoon. Anomalies at higher latitudes are considered to influence variations in the Asian monsoon (Yasunari 1986; Kripalani et al. 1997; Fujinami and Yasunari 2004; Ding and Wang 2007; Schiemann et al. 2007; Wang et al. 2008; Krishnan et al. 2009).

Fujinami and Yasunari (2004) showed that the intraseasonal anomaly along the subtropical jet induces a change in vertical motion over the Tibetan Plateau during the mature phase of the summer monsoon. This change affects the transportation of water vapor to the South Asian monsoon, causing the monsoonal activity to fluctuate.

Based on numerical experiments, Wang et al. (2008) suggested that enhanced diabatic heating on the Tibetan Plateau is responsible for the excitation of Rossby waves that propagate along the subtropical jet; additionally, their Fig. 3 shows wave propagation in the lower level, although this aspect was not discussed in detail in their paper. It is less well known that wave propagation also occurs in the lower level along the southwesterly monsoon flow. The

Corresponding author address: T. Watanabe, Graduate School of Environmental Science, Hokkaido University, Kita 10, Nishi 5, Kita-ku, Sapporo, Hokkaido 060-0810, Japan.
E-mail: nabetake@ees.hokudai.ac.jp

DOI: 10.1175/JCLI-D-11-00036.1

propagations of these wave trains to East Asia must also influence precipitation in this region.

Though the above-mentioned studies reported the influence of anomalies over the Tibetan Plateau on the Asian monsoon, others have considered the importance of anomalies over central Asia and over the western Tibetan Plateau. For example, Ding and Wang (2007) showed that the intraseasonal anomaly over central Asia, which is embedded in the subtropical jet, interacts with the activity of the South Asian monsoon. Based on numerical experiments, Krishnan et al. (2009) reported that the cyclonic anomaly over west-central Asia and the India–Pakistan region, which appears during the monsoon break, causes a linkage between the monsoon and midlatitude regions, which affects the monsoon flow. Furthermore, Murakami and Ding (1982) suggested that upper-tropospheric heating over the Afghanistan–western Tibetan Plateau region may be a prerequisite for the establishment of the summer monsoon near India.

The above-mentioned studies indicated that monsoonal activity is influenced by anomalies in the subtropics and midlatitudes. It seems that central Asia–western Tibetan and the central Tibetan Plateau are regions of contrasting processes in terms of influencing the activity of the Asian monsoon. Furthermore, the above-mentioned studies indicate that this influence occurs indirectly rather than directly, suggesting in turn that several mechanisms contribute to the linkage between higher-latitude regions and the Asian monsoon, although this point remains poorly understood.

As suggested by Murakami and Ding (1982), it would be interesting to focus on the transition phase of the summer Asian monsoon. In summer, larger interannual variability in the upper-level height field is seen over the region between central Asia and the western Tibetan Plateau (Ding and Wang 2005). Yanai et al. (1992) showed that warming over the region from Iraq to the western Tibetan Plateau is related to the development of a 200-hPa anticyclone over this region during the summer monsoon onset. These results highlight the need to focus on the intraseasonal anomaly over the Afghanistan–western Tibetan Plateau region in seeking to understand the monsoon condition during the transition phase of the summer Asian monsoon.

The purpose of the present study is to better understand the influence of higher-latitude anomalies on the Asian summer monsoon, considering the period of early summer (May–June). To this end, we examine the mechanisms that link higher-latitude intraseasonal anomalies with the Asian summer monsoon circulation, based on composite analyses of daily time series.

The remainder of the manuscript is organized as follows. Section 2 describes the data and analysis method used in this study, and section 3 presents the characteristics of upper- and lower-level circulations in early summer. Section 4 defines the geopotential height (GPH) index as the daily GPH anomaly at 200 hPa over Afghanistan and the western Tibetan Plateau, which represents variability of the upper-level disturbance, and section 5 presents the results of a composite analysis, anomalous circulations associated with the upper-level disturbance. Sections 6 and 7 consider the mechanisms through which higher-latitude anomalies influence the Asian summer monsoon. In section 6, the propagation of Rossby waves in lower-level westerlies is discussed based on the Rossby ray-path theory. Section 7 describes the development of the heat low caused by the upper-level anticyclonic anomaly over Afghanistan and the western Tibetan Plateau. Finally, conclusions and closing remarks are presented in section 8.

2. Data and analysis method

a. Data

We analyzed 6-hourly reanalysis data on a 2.5° × 2.5° grid, provided by the 40-yr European Centre for Medium-Range Weather Forecasts (ECMWF; ERA-40; Uppala et al. 2005) for May–June during 1958–2002. The analyzed variables are zonal and meridional wind velocities, vertical p velocity, geopotential height, and temperature at all levels (surface to 100 hPa). For most of the analyses, we use daily averaged data to remove diurnal variability.

Because May–June falls within the transition phase of the summer Asian monsoon (Wang and LinHo 2002), meteorological variables show increasing or decreasing trends during this period. We are interested in large deviations from these seasonal trends. Accordingly, we computed the 1-day climatology from 1958 to 2002 and smoothed it using a 5-day running mean. Anomalies were then calculated as deviations from the smoothed 1-day climatology for each variable.

b. Analysis method

The main technique employed in this study is composite analysis. We define the GPH index as the geopotential height anomaly at 200 hPa averaged over the rectangular domain shown (in Fig. 2a; discussed in detail in section 4). A positive GPH index indicates an upper-level anticyclonic disturbance.

We then identified the key days when the normalized GPH index exceeds +1.5. In the case that the interval between two key days was less than 10 days, the day with the larger index value was selected. This procedure was repeated until all the key days were separated by more than 10 days. Ultimately, we selected 35 key days over

TABLE 1. List of key days.

1 May 1959	3 Jun 1959	17 May 1960	9 May 1961	3 Jun 1961
2 Jun 1963	5 May 1966	16 Jun 1966	9 Jun 1967	28 May 1969
18 May 1970	26 Jun 1970	9 Jun 1971	13 Jun 1973	17 Jun 1975
6 Jun 1978	22 Jun 1980	2 May 1981	7 Jun 1982	14 Jun 1984
5 May 1986	6 Jun 1987	14 May 1990	22 Jun 1990	15 Jun 1991
10 Jun 1993	20 Jun 1994	13 May 1995	22 Jun 1996	16 May 1998
28 Jun 1998	9 May 1999	8 May 2000	12 May 2001	11 May 2002

a period of 45 yr (Table 1); some years have more than one key day and some have no key days.

The composite with respect to the key days of a variable is called day 0, and the time series of composites is computed for the 10 days either side of the key day. The composite of X days before/after the key day is referred to as day $\pm X$.

3. Characteristics of upper- and lower-level circulations in early summer

Figure 1 shows the climatologies of the horizontal wind vector and the zonal wind velocity for the 2-month period of May–June at 200 and 850 hPa. At 200 hPa, a strong westerly wind occurs along the 30°–40°N band over Afghanistan and the Tibetan Plateau (Fig. 1a). The westerly jet axis is located at about 200 hPa during this season (Schiemann et al. 2009). The center of the jet is located at approximately 35°N in May and at approximately 40°N in June, moving northward with the march of the South Asian summer monsoon. Hoskins and Ambrizzi (1993) reported that the westerly jet can act as a Rossby waveguide, with Rossby waves propagating while trapped in the waveguide. Therefore, it is expected that anomalies in the extratropics would commonly propagate eastward over the study region in the form of a Rossby wave along the waveguide.

At 850 hPa, a belt of stronger westerlies occurs locally from south of the Arabian Sea to south of the Bay of Bengal (Fig. 1b). The strength and distribution of these westerlies vary with the activity of the South Asian monsoon (Joseph and Sijikumar 2004). The westerly belt has an easterly vertical shear and the westerly reaches its maximum at around 850 hPa.

4. Definition of the GPH index

Figure 2a shows the distribution of the root-mean-square of anomalous geopotential height at 200 hPa for the 2-month period May–June during 1958–2002. Following the computational procedure, the root-mean-square includes both intraseasonal and interannual variations, though the intraseasonal variation is dominant. Large values are seen over Afghanistan and the western Tibetan Plateau (herein referred to as the ''AWTP region''), corresponding to the location of the westerly jet. Ding and Wang (2005) reported large variability for a similar region to that analyzed in the present study, although they considered interannual variability in the mature phase of the summer monsoon. Previous studies have also suggested that upper-level anomalies in this region have an intraseasonal influence on the Asian monsoon (Fujinami and Yasunari 2004; Ding and Wang 2007; Krishnan et al. 2009).

An analysis of geopotential height anomalies in this region would provide clues to the nature of the link between the extratropics and the Asian monsoon. Thus, we define the index in such a way that it represents fluctuations in the height field. The rectangle over the AWTP region (30°–40°N, 60°–75°E) in Fig. 2a represents the region in which the index is defined, located along the propagation path of anomalies in the extratropics during the transition phase of the summer Asian monsoon.

In section 7, we discuss the subtropical region around 70°E, consisting of the eastern Iranian Plateau, the western Tibetan Plateau, and the Thar Desert (Fig. 2b). The western part of the region is the eastern margin of the Plateau of Iran, at an elevation of about 2000 m. The eastern part of the region is the Thar Desert—a lowland area. Herein, the Thar Desert and neighboring areas (25°–30°N, 62.5°–72.5°E) are collectively referred to as the ''TD region,'' which is presented as a rectangular domain in Fig. 2b. These areas are all arid (Kottek et al. 2006). In summer, a thermal low is maintained over this region (Slingo 2003), which is bounded to the north by mountain ranges of the western Tibetan Plateau, such as the Hindu Kush and the Karakoram. Herein, these two mountain ranges are collectively referred to as the ''H–K mountain ranges''.

5. Results of composite analysis

Figure 3 shows a time series of composites of the anomalous horizontal wind and anomalous vorticity tendency in the upper level (200 hPa) and lower level (850 hPa). A positive (negative) anomalous vorticity tendency corresponds to the strengthening of cyclonic circulation or the weakening of anticyclonic circulation (weakening of cyclonic circulation or strengthening of anticyclonic

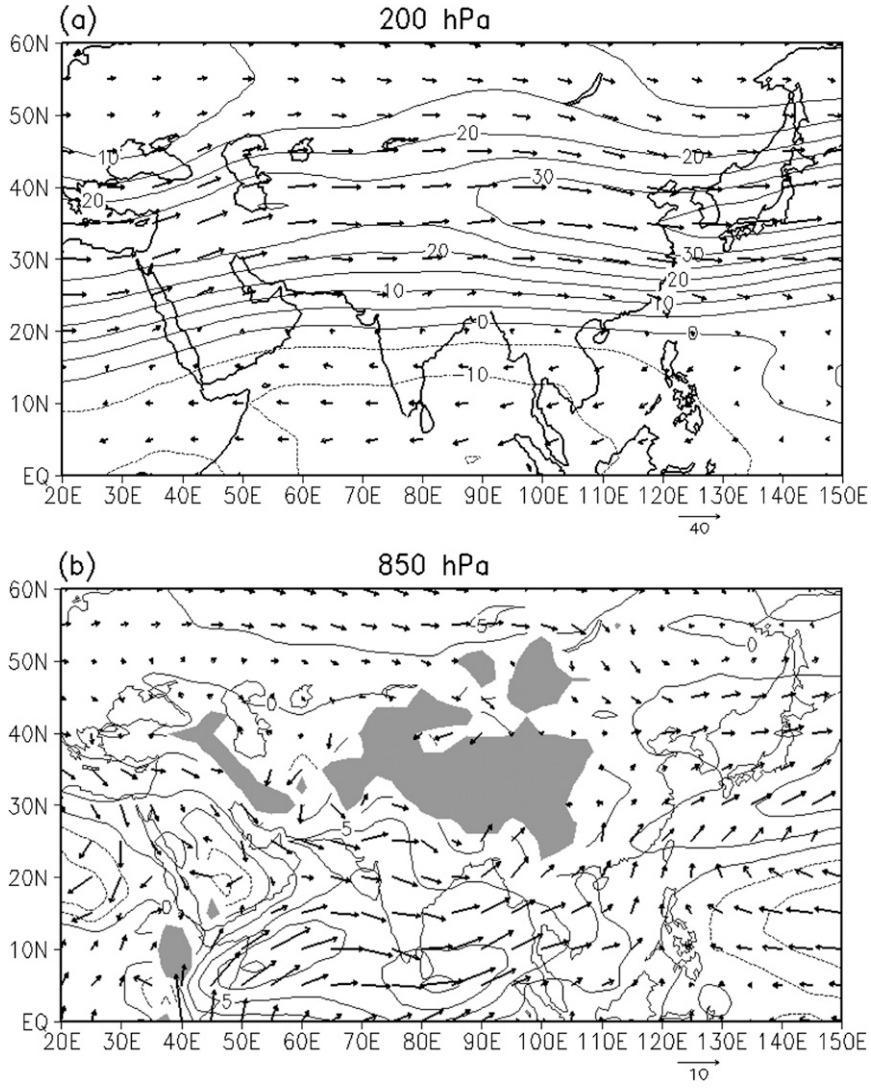

FIG. 1. Climatologies of horizontal wind (vectors; m s^{-1}) and zonal wind velocity (contours) for the 2-month period May–June at (a) 200 and (b) 850 hPa. The contour interval is 5 m s^{-1} in (a) and 2.5 m s^{-1} in (b). Dotted contours indicate negative values. Shaded area in (b) represents topography above 1500 m.

circulation). An eastward-propagating anomaly is apparent at each level. The following discussion focuses on these anomalies.

In the upper level, a strong anticyclonic anomaly is found over the AWTP region at day 0 (Fig. 3b), centered over the region in which the GPH index is defined. Cyclones occur to the west and east of the anticyclone. A cyclone to the northwest is weakening at day 0, whereas to the east, over China, a cyclone is strengthening. Farther east, an anticyclone is being generated over the Japan islands. Those anomalies show a wave train pattern along the subtropical jet at about 35°N (Fig. 1a).

The anomalous vorticity tendency over the AWTP region has a negative value at day −2, which indicates strengthening of the anticyclonic circulation (Fig. 3a), which is developed after day −4 (not shown) and attains a maximum at day 0 (Fig. 3b), subsequently weakening and moving slowly eastward (Figs. 3c and 3d).

The anomalous cyclonic circulation to the northwest of the AWTP region is generated before the formation of the anticyclone over the AWTP region. The strength of the anomalous cyclone attains a maximum at day −1 and weakens thereafter. It is located over the northwest of the Caspian Sea (50°N, 45°E) before day −4 and subsequently moves to the southwest. The cyclone over China attains a maximum at day +2. Unlike the other vortices, the anomalous anticyclonic circulation over the Japan islands does not strengthen. We examined all the members

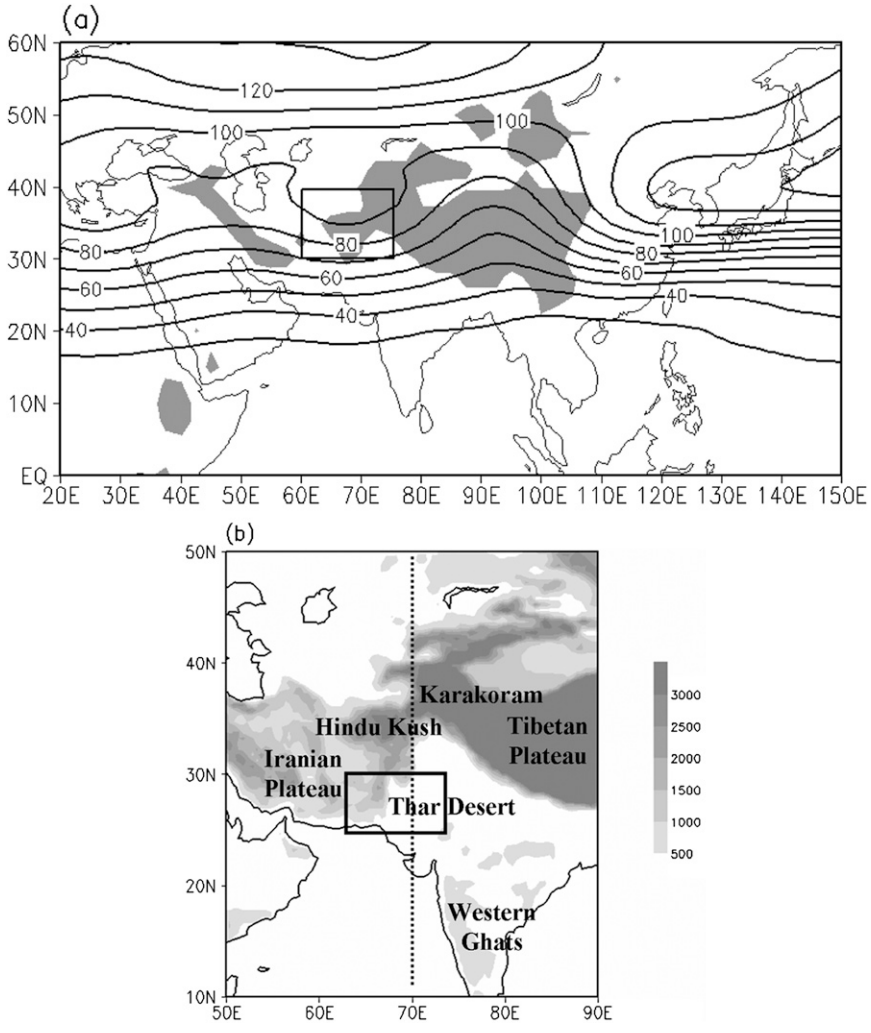

FIG. 2. (a) Distribution of the root-mean-square of anomalous GPH at 200 hPa for the 2-month period May–June during 1958–2002. Contour interval is 10 m. The rectangle (30°–40°N, 60°–75°E) indicates the region in which the GPH index is defined. Shaded area represents topography above 1500 m. (b) Topography of the main regions analyzed in section 7. Shading represents altitude (m). The rectangle (25°–30°N, 62.5°–72.5°E) indicates the TD region (Thar Desert and neighboring areas). Dotted line indicates a longitude of 70°E.

and found that failure to strengthen occurs because each composite member has a slightly different wavelength and their phases are not completely consistent with each other.

The wavelength of the anomaly is about 65° in longitude at 35°N, as estimated from the interval between vortices. The group velocity is estimated to be 32° day^{-1}, based on the interval of days when the strength of each vortex attains a maximum. The direction of propagation is eastward along the westerly jet centered at about 35°N. This propagation pattern of the anomaly is similar to that observed in summer along the North African–Asian jet, which is called the Silk Road pattern (Hoskins and Ambrizzi 1993; Enomoto et al. 2003). Kosaka et al. (2009) suggested the pattern is fixed geographically by barotropic energy conversion over the Caspian Sea. The upper-level anomaly propagates from the Caspian Sea and seems to be generated by the same energy conversion.

Another anomaly, propagating eastward from the Arabian Sea between 10° and 20°N, is apparent in the lower level. At day +2, we see an anomalous cyclonic vortex from the north of the Arabian Sea to the TD region and an anomalous anticyclonic vortex over the region from the southeast of the Arabian Sea to the Indian subcontinent (Fig. 3g), along with an anomalous cyclonic vortex over the Bay of Bengal. The anomalous vorticity tendency has a positive value over the central Bay of Bengal at day +2; consequently, an anomalous cyclonic

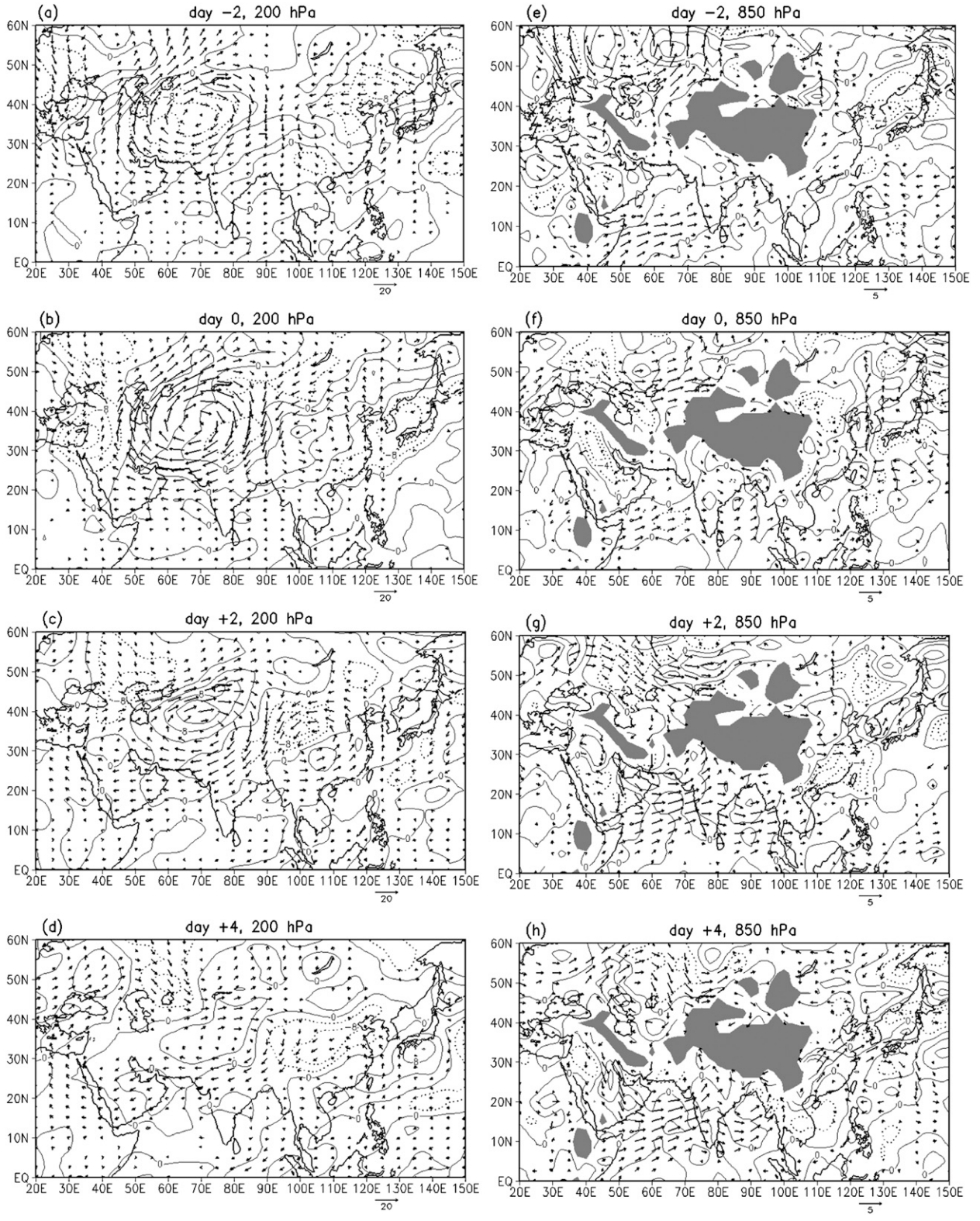

FIG. 3. Composites of the anomalous horizontal wind (vectors; m s^{-1}) and the anomalous vorticity tendency (contours) at day −2, day 0, day +2, and day +4 at (a)–(d) 200 and (e)–(h) 850 hPa. Vectors are plotted only where statistically significant at the 95% level. Contour intervals are 4×10^{-6} s^{-2} at 200 hPa and 1×10^{-6} s^{-2} at 850 hPa. Solid (dotted) lines represent positive (negative) values, which show where cyclonic (anticyclonic) circulation is developed.

vortex develops. A cyclonic anomaly develops over the north of the Bay of Bengal and the mouth of the Ganges at day −2 and day 0 (Figs. 3e and 3f); however, when the anomaly begins to propagate, an anomalous cyclonic circulation develops south of the preexisting cyclonic anomaly, over the center of the Bay of Bengal, along the path of propagation. At day +4, the anomalous vorticity tendency has a negative value over the Indochina Peninsula and the western South China Sea (east of the cyclonic anomaly over the Bay of Bengal), indicating the development of an anticyclonic anomaly (Fig. 3h) that attains a maximum during days +5 and +6. The anomaly then reaches the Philippines at day +7 and generates a cyclonic anomaly (not shown), although the circulation pattern is not apparent farther east. This pattern of wave train is stationary until day +4. Subsequently, the vortices weaken from the west, with the wavy pattern becoming unclear and showing a gradual collapse. The anomaly propagates eastward from the Arabian Sea to the Philippines over a period of about 5 days, along the strong westerly belt (Fig. 1b).

The lower-level anomalous circulation first appears along 70°E over the region from the north of the Arabian Sea to the TD region. The anomalous west-southwesterlies are generated between two vortices, and intensify with strengthening of the vortices. At day −2, anomalous west-southwesterlies are apparent over the southern Arabian Sea and blow toward the southern tip of the Indian subcontinent (Fig. 3e). The anomalous west-southwesterly wind shows a rapid strengthening and spreads to the north of the Arabian Sea at day 0. The region of maximum velocity changes from the southwest to the northeast of the Arabian Sea. At day +2, the strength of the anomalous southwesterly wind, which blows around the southern part of the cyclonic anomaly over the region from the north of the Arabian Sea to the TD region, attains a maximum and the anomalous wind blows toward the west coast of the Indian subcontinent. At the same time, the anomalous southwesterly wind blows over the Thar Desert toward the H–K mountain ranges (Fig. 3g). These anomalous winds are maintained until day +5.

Other interesting phenomena at the low-level are seen over two areas: East Asia and the area around the Tibetan Plateau. Over East Asia, a prominent anomalous wind blows from the southwest and west-southwest over the southern part of China, the South China Sea, and the area west of the Japan islands after day +2, and it is maintained until day +6 (Figs. 3g and 3h, although data are only shown up to day +4). Given that the lower-level anomaly starts from the Arabian Sea at day +2, the anomalous wind over East Asia appears to be influenced by the upper-level cyclonic anomaly over China (Figs. 3c and 3d). After the lower-level anomaly reaches the Indochina Peninsula, an anticyclone is generated in this region. At the same time, the anomalous southwesterlies spread to the northwest of the Indochina Peninsula and coastal areas of the western South China Sea (not shown). Therefore, this anomalous southwesterly wind also appears to be influenced by the lower-level anomaly.

Between day 0 and day +2, the anomalous anticyclonic circulation is clearly developed around the Tibetan Plateau. At higher levels, a similar circulation is seen around the Tibetan Plateau, although stronger and more pronounced than that at lower levels. This circulation is probably generated by the interaction between the developed upper-level anticyclonic anomaly and the topography of the Tibetan Plateau. These phenomena are of interest but are not discussed in greater detail in the present study.

We found the observed signature of the lower-level propagating anomaly, which is similar to that obtained by Wang et al. (2008) in a numerical simulation. Though they suggested that the upper-level anticyclonic anomaly, which is forced by heating over or on the Tibetan Plateau in summer, generates the lower-level anomaly, no details were provided. The propagation of the lower-level anomaly is discussed in detail in section 6 below.

6. Propagation of the low-level anomaly

Figure 4 shows a longitude–time diagram of anomalous vorticity along 15°N at 850 hPa. The alternating generation of anticyclonic and cyclonic anomalies is seen to propagate eastward over time. The anomalous vortices extend eastward from the southeast of the Arabian Sea/Indian subcontinent at 70°E (day +2) to the Bay of Bengal at 85°E (day +4), to the Indochina Peninsula at 105°E (day +6), and to the Philippines at 120°E (day +7). The vorticity anomalies are quasi stationary, and each vortex is maintained for about 4 days.

The bold line in Fig. 4 represents the propagation path of the lower-level anomaly. The average propagation speed (group velocity) is 10° day^{-1} (about 12 m s^{-1}), and the average wavelength is about 3700 km (wavenumber of about 10).

The Rossby ray-path theory (Hoskins and Ambrizzi 1993) is applied to the region with strong low-level westerlies. According to the theory, the stationary wavenumber is defined as follows:

$$K = \left(\frac{\beta_*}{\overline{U}}\right)^{1/2}, \tag{1}$$

where

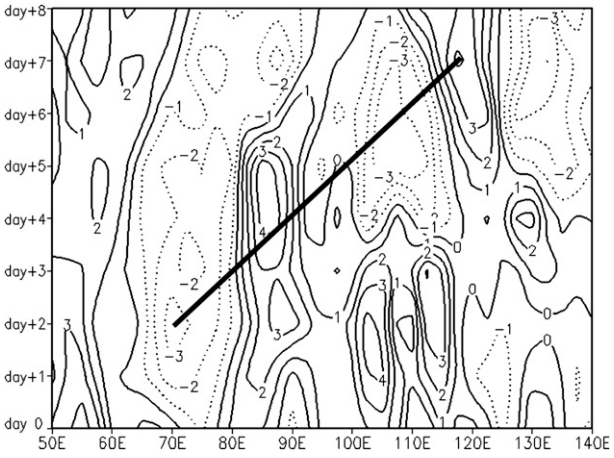

FIG. 4. Longitude–time diagram of the anomalous vorticity along 15°N at 850 hPa. Contours represent anomalous vorticity with a contour interval of 1×10^{-6} s^{-1}. Bold line represents the propagation path of the anomaly.

$$\beta_* = \beta - \frac{\partial^2 \overline{U}}{\partial y^2} \tag{2}$$

is the meridional gradient of absolute vorticity.

A strong westerly belt, in which the absolute vorticity shows strong meridional variability, acts as a Rossby waveguide (Hoskins and Ambrizzi 1993). The waveguide has a unique distribution of stationary Rossby wavenumber, whereby a zonal belt of higher total wavenumber is sandwiched by zonal belts of lower total wavenumber. The Rossby wave propagates in the Rossby waveguide, refracted toward latitudes with a higher wavenumber.

Figure 5a shows the average composite of the actual zonal wind from day +2 to day +6 at 850 hPa, and Fig. 5b shows the total stationary wavenumber K, calculated from the actual zonal wind in Fig. 6a. Strong westerlies, exceeding 8 m s^{-1}, occur over the Arabian Sea and the Bay of Bengal between 5° and 20°N. The path of the anomalous vorticity follows this strong westerly belt.

Figure 5b shows that the distribution of the zonal belt with a high total wavenumber is sandwiched by zonal belts with a low total wavenumber, which is typical for a waveguide. The stationary wavenumber over the waveguide is about 10, which corresponds well to the observed wavenumber. It appears that the strong westerly belt acts as a waveguide, and that the low-level anomaly propagates eastward along the waveguide in the form of a quasi-stationary Rossby wave.

7. Mechanisms that explain the influence of the upper-level anomaly on the lower-level anomaly

With the initial propagation of the lower-level anomaly, the southwesterly wind over the Arabian Sea, accompanied

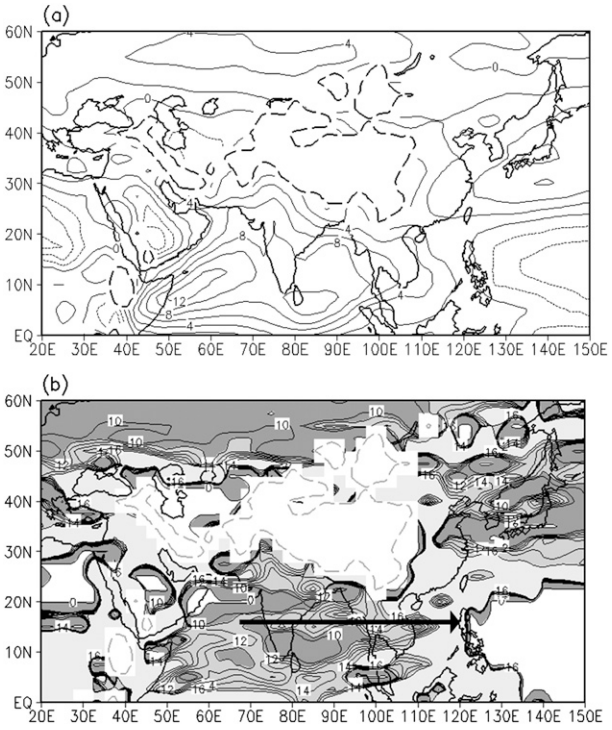

FIG. 5. (a) Average composite of the actual zonal wind velocity between day +2 and day +6 at 850 hPa. Contours represent the zonal wind speed with a contour interval of 2 m s^{-1}. (b) The total stationary Rossby wavenumber was calculated from (a). Contours represent the wavenumber. Only values between 10 and 16 are drawn, with a contour interval of 1. Darker shading indicates smaller wavenumbers. No shading indicates areas where the stationary Rossby wave cannot exist. Thick line with an arrowhead shows the possible waveguide.

by the cyclonic anomaly over the TD regions, is strengthened (Fig. 3g). The findings of Gadgil (1977) indicate that this strong anomalous southwesterly is likely to cause the anticyclonic anomaly over the Indian subcontinent through its interaction with topography, that is, the Western Ghats, which are oriented north–south and have an average elevation of 1200 m. The situation for

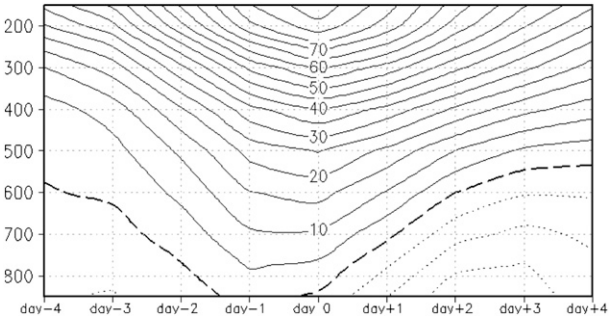

FIG. 6. Time–pressure diagram for the composite of anomalous GPH averaged over the TD region. Contour interval is 5 m.

a westerly flow impinging on a topographic barrier is shown in Fig. 4.9 of Holton (2004). In this figure, the anticyclonic flow pattern appears to the east side of the mountain barrier, followed by an alternating series of ridges and troughs downstream. This pattern arises because the vertical extent of air columns in the westerly decreases over the mountain barrier, resulting in reduced relative vorticity. Thus, the air columns acquire an anticyclonic vorticity.

The Western Ghats likely act as the barrier, interacting with the columns in the southwesterly flow. To conserve the absolute vorticity, an anticyclonic anomaly appears over the Indian subcontinent, followed by the start of eastward propagation of the lower-level anomaly in the waveguide. Thus, the development of the cyclonic anomaly over the TD region is considered to cause the subsequent eastward propagation of the lower-level Rossby wave. The remainder of this section examines how the lower-level cyclonic anomaly over the TD region is associated with the upper-level anticyclonic anomaly.

Figure 6 shows a time–pressure diagram for the composite of anomalous geopotential height averaged over the TD region. Until day −1, an increase in anomalous geopotential is seen at all levels. In the upper and mid-levels, anomalous geopotential height increases until day 0, whereas it starts decreasing in the lower level after day −1 and the negative geopotential height anomaly shows rapid development. The negative geopotential height anomaly attains a maximum in the lowest level at day +2, two days after the maximum anticyclonic anomaly in the upper level at day 0, corresponding to the appearance of a cyclonic anomaly over the TD region (see Fig. 3g). The development of the low is evident in the composite pressure field (not shown).

Figure 7 shows latitude–pressure cross sections along 70°E for composites of anomalous meridional and vertical wind vectors and anomalous temperature at day 0 and day +2. The region along 70°E passes through the Arabian Sea, the TD region, and the H–K mountain ranges. This region contains the center of the upper-level anticyclonic anomaly (Fig. 3b) and the lower-level cyclonic anomaly, as well as the lower-level anomalous wind that blows toward the H–K mountain ranges over the Thar Desert (Fig. 3g).

At day 0, strong anomalous descent is evident over the H–K mountain ranges between 30° and 40°N (Fig. 7a). To the south, anomalous descent is observed between the mid- and lower levels, along the slopes of the H–K mountain ranges. These anomalous descents appear at day −4 and are strengthened with the development of the upper-level anticyclonic anomaly.

The vertical distribution of anomalous circulation shows a marked change from day 0 to day +2. At day +2, the pronounced anomalous descent over the H–K mountain ranges disappears (Fig. 7b). Anomalous ascents are generated in the upper level to the north and south of the H–K mountain range but thereafter show a rapid decline. In the lower level, a southwesterly anomaly is seen over the TD region, which is maintained until day +5 and is accompanied by a cyclonic anomalous vortex over the TD region (Fig. 3g) that appears only in the lower level.

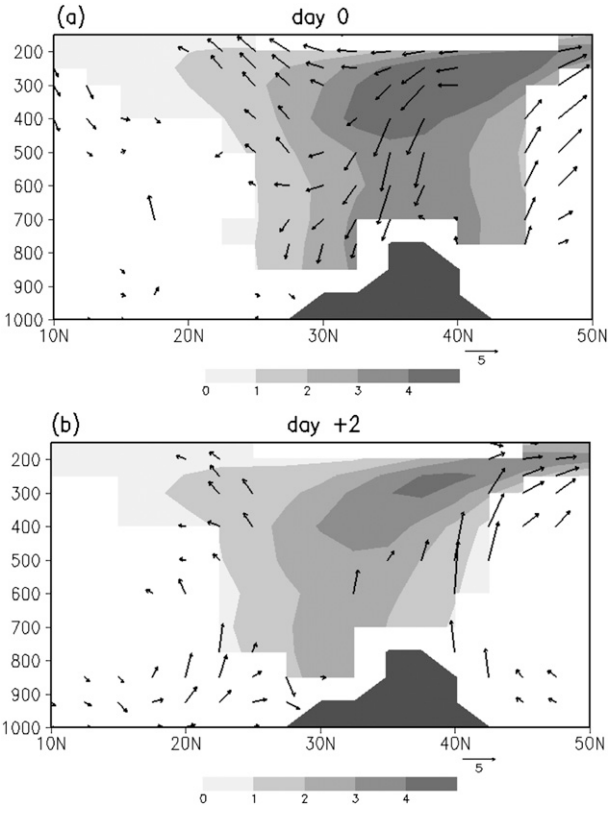

FIG. 7. Latitude–pressure cross sections along 70°E for composites of anomalous meridional and vertical wind (vectors), and anomalous temperature (shading) at (a) day 0 and (b) day +2. Vectors are plotted only where meridional zonal and/or vertical wind components are statistically significant at the 95% level. The unit of meridional wind speed is m s^{-1}. The unit of vertical wind is Pa s^{-1}, and the vertical wind component is multiplied by −100. Dark shading at the bottom of each panel represents the topography.

At day 0, a higher-temperature anomaly is located over the H–K mountain ranges in the upper level (Fig. 7a), associated with the upper-level anticyclonic anomaly. The higher-temperature anomaly between the mid- and lower levels, which is almost uniform vertically, corresponds to anomalous descent (Fig. 7a). Therefore, adiabatic heating, strengthened by anomalous descent, causes an increase in temperature at the mid- and lower levels.

Figure 8 shows latitude–pressure cross sections for composites of the actual meridional-vertical wind vector

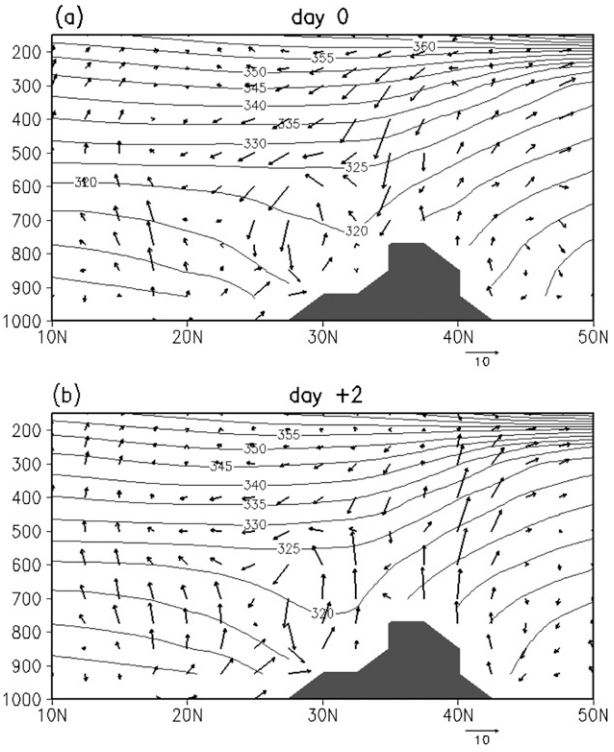

FIG. 8. Latitude–pressure cross sections along 70°E for composites of actual meridional–vertical wind (vectors) and potential temperature (contours) at (a) day 0 and (b) day +2. The unit for meridional wind speed is m s^{-1}. The unit for vertical wind is Pa s^{-1}, and the vertical wind component is multiplied by −100. Contours represent potential temperature with a contour interval of 10 K. Shaded area between 25° and 45°N at the bottom of each panel denotes the topography.

and potential temperature along 70°E at day 0 and day +2. In the actual circulation, descent is prominent over the H–K mountain ranges in the upper level, at both day 0 and day +2. The descents are strengthened by anomalous descent at day 0 (Fig. 8a) but weakened by the disturbance of anomalous ascent at day +2 (Fig. 8b). Overturning circulation is apparent south of the H–K mountain ranges, below 500 hPa. The descent is stronger on the south side of the circulation at day 0, whereas the ascent on the north side and southerlies at the bottom of the circulation are stronger at day +2. Stronger ascent is also seen around 20°N at the lower level. The above change between day 0 and day +2 shows that the anomalous circulation has a strong influence on the actual circulation. However, the upper-level descent is maintained during this period, suggesting that deep convection is prevented and that cloudless weather is maintained. At around 30°N, an area with higher potential temperature is observed at day 0 and day +2. The vertical gradient of potential temperature is less steep in this area. Consequently, the development of a mixed boundary layer is expected, with its top located between 500 and 600 hPa.

Given the topographic and atmospheric conditions, it is supposed that the development of the anomalous low over the TD region is similar to that of a heat low (Blake et al. 1983; Smith 1986), which can be observed in a shallow layer at the bottom of the deeply developed mixed layer over desert areas. Blake et al. (1983) and Smith (1986) demonstrated that the heat low over the Saudi Arabian desert is generated from adiabatic heating associated with strong subsidence at all levels, solar heating in the lower level, and near-surface sensible heating.

Blake et al. (1983) showed that the heat low has a large diurnal cycle, in which lower-level upward motion is enhanced during daytime, and that adiabatic heating associated with strong subsidence and near-surface sensible heating are important factors in the development of the heat low. To examine the thermal structure of the anomalous low over the TD region, a thermodynamic equation is applied to the 6-hourly data of each composite member, and composites are calculated for each term in the thermodynamic equation. Figure 9 shows the vertical distributions of composites of terms in the thermodynamic equation, namely, horizontal advection, vertical advection, and the residual, which includes diabatic heating, averaged for each period between day 0 and day +4 over the Thar Desert (25°–30°N, 67.5°–72.5°E). The diabatic term shows heating at 1100, 1700, and 2300 local time (LT) in the lower level and attains a maximum at the lowest level (Figs. 9b–d), though the signal is weak at 2300 LT. However, the diabatic term is negative at 0500 LT (Fig. 9a). Strong daytime diabatic heating occurs only near the surface, probably because of sensible heating from the surface. The adiabatic heating due to vertical advection is dominant in the midlevel. The adiabatic term is negative in the lower level at 1100 and 1700 LT because of the ascent that accompanies the low over the TD region, though the adiabatic term shows heating at 0500 LT. These terms are stronger than the climatology (not shown). Near-surface diabatic heating under cloudless conditions contributes to the development of the heat low during the day, whereas it declines under the influence of diabatic cooling at night. This finding indicates that the anomalous low over the TD region has the same structure as the heat low, and that strengthening of the anomalous descent from the upper level to the midlevel is important for the development of the heat low in the lower level.

To identify the origin of the change in vertical motion, the **Q** vector is used to diagnose the vertical motion. The **Q** vector diagnoses vertical motion due to adiabatic flow in the ω equation, under quasigeostrophic theory (Hoskins et al. 1978), and can be computed from temperature and

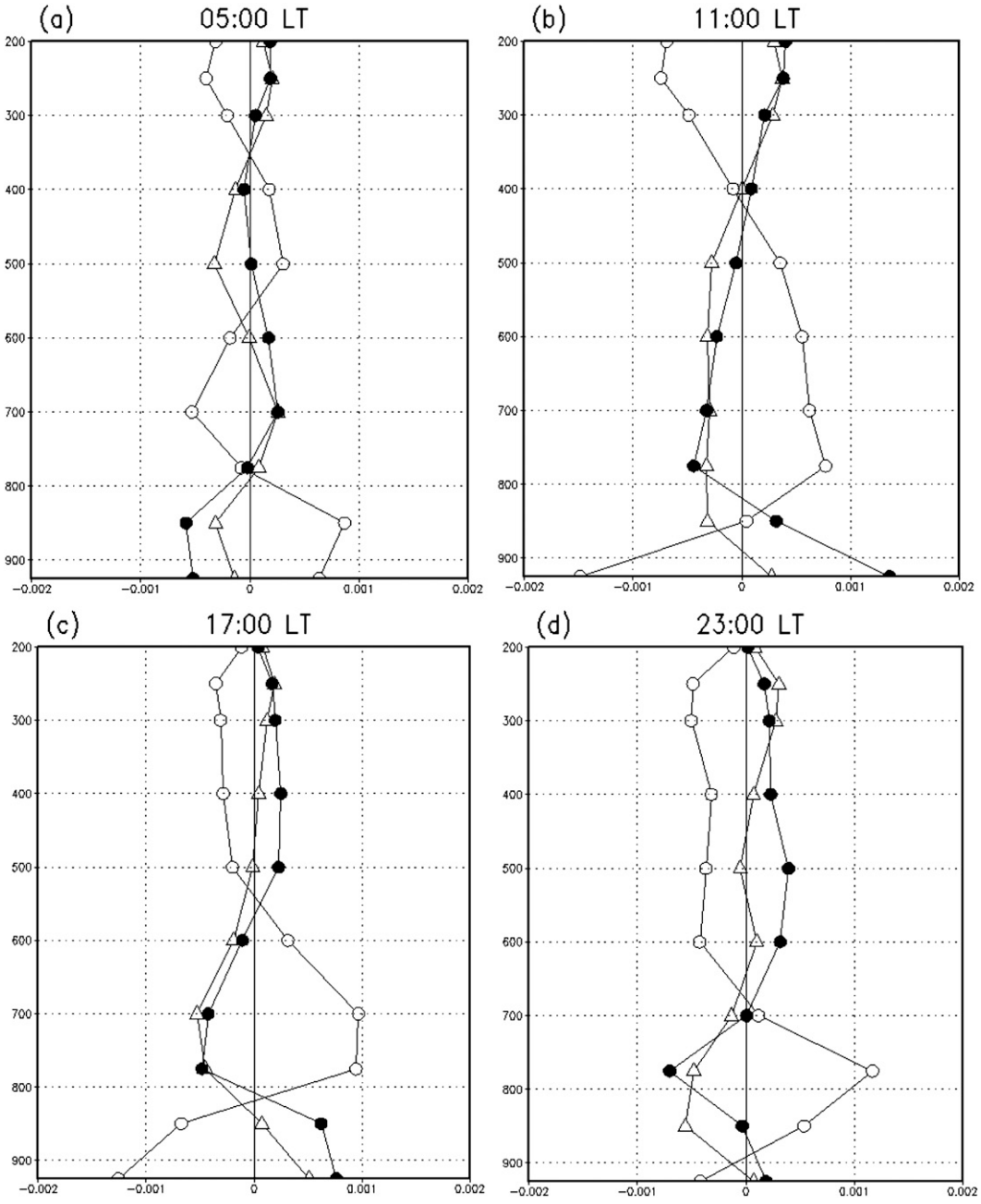

FIG. 9. Vertical distributions of composites of terms in the thermodynamic equation averaged over the Thar Desert (25°–30°N, 67.5°–72.5°E) at (a) 0000 UTC (0500 LT), (b) 0600 UTC (1100 LT), (c) 1200 UTC (1700 LT), and (d) 1800 UTC (2300 LT). Triangles denote horizontal advection, open circles denote vertical advection, and closed circles denote the residual, which includes diabatic heating (K s^{-1}).

height fields. The divergence/convergence of the **Q** vector indicates dynamically forced descent/ascent by a geostrophic motion.

Figure 10 shows composites for the anomalous vertical p velocity and the **Q** vector with respect to the anomalous field at 400 hPa at day 0. This anomalous **Q** vector is defined as the difference between 1) the **Q** vector with respect to the actual composites fields and 2) that with respect to the climatological fields.

Midlatitude regions show a good correspondence between divergence/convergence of the **Q** vector and the positive/negative vertical p velocity. The anomalous descent (ascent) to the east (west) of the anticyclonic anomaly corresponds to divergence (convergence) of the **Q** vector.

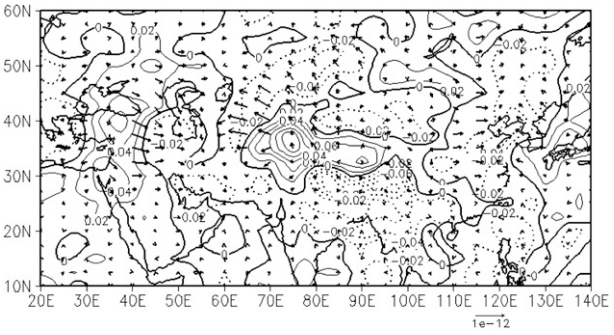

FIG. 10. Composites for anomalous vertical p velocity (contours; Pa s^{-1}) and the **Q** vector for the anomalous field (vectors; kg^{-1} m^2 s^{-1}) at 400 hPa at day 0.

A similar correspondence is also seen down to 700 hPa (not shown). Therefore, the anomalous descent along 70°E is generated by the anticyclonic anomaly, directly and adiabatically.

8. Conclusions and remarks

We examined the influence of an anticyclonic anomaly in the subtropical jet on the intraseasonal variability of the Asian monsoon in early summer (May–June), which corresponds to the transition phase of the summer Asian monsoon (Wang and LinHo 2002). To this end, the GPH index was defined as the daily geopotential height anomaly averaged over the AWTP region, which is characterized by large intraseasonal variability in the height field. We also calculated the composite with respect to a strongly positive GPH index, that is, a strong anticyclonic anomaly.

The results show that quasi-stationary anomalies propagate eastward in both the upper and lower levels. In the upper level, a strong anomalous anticyclonic vortex appears in the AWTP region at day 0 and the anomaly propagates eastward along the subtropical jet at about 35°N, toward the Japan islands. This propagation pattern of anomalies is similar to that observed in summer along the North African–Asian jet, which is called the Silk Road pattern (Hoskins and Ambrizzi 1993; Enomoto et al. 2003).

In the lower level, a cyclonic anomaly also appears from the TD region to the north of the Arabian Sea at day +2. The anomaly propagates eastward to the Indian subcontinent, the Bay of Bengal, and the Indochina Peninsula, reaching the Philippines at day +7. The anomaly is quasi stationary with a wavenumber of about 10. The propagation path of the anomaly is around 15°N, within the strong westerly belt.

We identified the following two mechanisms related to the propagation of the lower-level anomaly:

1) The Rossby ray-path theory (Hoskins and Ambrizzi 1993) was applied to the region with strong lower-level westerlies, indicating that the strong westerly belt acts as a waveguide and that the lower-level anomaly propagates eastward along it in the form of a stationary Rossby wave with a wavenumber of about 10.
2) An analysis employing the **Q** vector (Hoskins et al. 1978) indicated that the upper-level anticyclone generates anomalous descent over the TD region, directly and adiabatically. The upper-level anomalous anticyclone promotes the development of a heat low over the TD region, through adiabatic heating associated with strong subsidence and near-surface sensible heating. The heat low attains a maximum at day +2. The anomalous southwesterly associated with the heat low blows toward the western Indian subcontinent, where it interacts with the topographic barrier of the Western Ghats. An anticyclonic anomaly is generated over the Indian subcontinent, followed by the initial eastward propagation of the anomaly.

The present results indicate that the temporary anomaly in the subtropical jet influences the monsoon over South Asia, Southeast Asia, and probably also over East Asia. This influence arises from two main processes: eastward propagation of quasi-stationary anomalies in both the upper and lower levels. As the anomalies propagate eastward, increasing precipitation is seen over Bangladesh, Myanmar, and along the south side of the Tibetan Plateau (not shown). This result indicates that the change in circulation due to two quasi-stationary anomalies influences the Asian monsoon. Detailed results and a related discussion will be presented in a future study.

Finally, this study contributes to our understanding of the monsoon in the following three ways:

1) Although not shown in this study, the composite with respect to the strongly negative GPH index has a pattern that is almost opposite to that of the strongly positive GPH Index, though the intensity of the negative case is weaker than that of the positive case. Terao (1998) showed that intraseasonal variation in the subtropical jet is dominant at periods of 30–40 days and around 14 days in summer. It is possible that the intraseasonal variation in the subtropical jet influences the oscillation of activity of the Asian summer monsoon through the processes identified in the present study.
2) It is possible that the mechanisms identified in this study can be applied to explain the monsoon onset. The period considered in this analysis falls within the transition phase of the summer Asian monsoon. A temperature increase from the Iranian plateau to the Thar Desert, along with strong westerlies, is observed

at the onset of the summer Asian monsoon (Yanai et al. 1992; Zhang et al. 2004), which is similar to the phenomena observed in this study. This similarity suggests that upper-level anticyclonic anomaly may trigger a sudden onset and the active phase of the summer Asian monsoon.

3) Though this study is concerned with intraseasonal variability, the findings are likely to be applicable to interannual variability. The upper-level anticyclonic anomaly and the resultant anomalous lower-level westerly act to strengthen the westerly shear over the Arabian Sea (Fig. 3), which corresponds to a strong South Asian monsoon. The interannual anomaly over the western Tibetan Plateau may have an important effect on the intensity of the South Asian monsoon. Moreover, the mechanism that underlies the anomaly could be explained by the present findings.

Acknowledgments. We thank two anonymous reviewers and the journal editor for their valuable comments and suggestions that improved the manuscript. The authors also thank Drs. F. Hasebe and T. Horinouchi for their valuable suggestions regarding this study.

REFERENCES

Annamalai, H., and J. M. Slingo, 2001: Active/break cycles: Diagnosis of the intraseasonal variability of the Asian summer monsoon. *Climate Dyn.,* **18,** 85–102.

Blake, D. W., T. K. Krishnamurti, S. V. Low-Nam, and J. S. Fein, 1983: Heat low over the Saudi Arabian desert during May 1979 (summer MONEX). *Mon. Wea. Rev.,* **111,** 1759–1775.

Ding, Q., and B. Wang, 2005: Circumglobal teleconnection in the Northern Hemisphere summer. *J. Climate,* **18,** 3483–3505.

——, and ——, 2007: Intraseasonal teleconnection between the summer Eurasian wave train and the Indian monsoon. *J. Climate,* **20,** 3751–3767.

Duan, A. M., and G. X. Wu, 2005: Role of the Tibetan Plateau thermal forcing in the summer climate patterns over subtropical Asia. *Climate Dyn.,* **24,** 793–807.

Enomoto, T., B. J. Hoskins, and Y. Matsuda, 2003: The formation mechanism of the Bonin high in August. *Quart. J. Roy. Meteor. Soc.,* **129,** 157–178.

Fujinami, H., and T. Yasunari, 2004: Submonthly variability of convection and circulation over and around the Tibetan Plateau during the boreal summer. *J. Meteor. Soc. Japan,* **82,** 1545–1564.

Gadgil, S., 1977: Orographic effects on the southwest monsoon: A review. *Pure Appl. Geophys.,* **115,** 1413–1430.

Holton, J. R., 2004: *An Introduction to Dynamic Meteorology*. 4th ed. Elsevier, 535 pp.

Hoskins, B. J., and T. Ambrizzi, 1993: Rossby wave propagation on a realistic longitudinally varying flow. *J. Atmos. Sci.,* **50,** 1661–1671.

——, I. Draghici, and H. C. Davies, 1978: A new look at the ω-equation. *Quart. J. Roy. Meteor. Soc.,* **104,** 31–38.

Joseph, P. V., and S. Sijikumar, 2004: Intraseasonal variability of the low-level jet stream of the Asian summer monsoon. *J. Climate,* **17,** 1449–1458.

Kosaka, Y., H. Nakamura, M. Watanabe, and M. Kimoto, 2009: Analysis on the dynamics of a wave-like teleconnection pattern along the summertime Asian jet based on a reanalysis dataset and climate model simulations. *J. Meteor. Soc. Japan,* **87,** 561–850.

Kottek, M., J. Grieser, C. Beck, B. Rudolf, and F. Rubel, 2006: World map of the Köppen-Geiger climate classification updated. *Meteor. Z.,* **15,** 259–263.

Kripalani, R. H., A. Kulkarni, and S. V. Singh, 1997: Association of the Indian summer monsoon with the Northern Hemisphere mid-latitude circulation. *Int. J. Climatol.,* **17,** 1055–1067.

Krishnan, R., V. Kumar, M. Sugi, and J. Yoshimura, 2009: Internal feedbacks from monsoon–midlatitude interactions during droughts in the Indian summer monsoon. *J. Atmos. Sci.,* **66,** 553–578.

Murakami, T., and Y.-H. Ding, 1982: Wind and temperature changes over Eurasia during the early summer of 1979. *J. Meteor. Soc. Japan,* **60,** 183–196.

Randel, W. J., and M. Park, 2006: Deep convective influence on the Asian summer monsoon anticyclone and associated tracer variability observed with Atmospheric Infrared Sounder (AIRS). *J. Geophys. Res.,* **111,** D12314, doi:10.1029/2005JD006490.

Rodwell, M. J., and B. J. Hoskins, 1996: Monsoons and the dynamics of deserts. *Quart. J. Roy. Meteor. Soc.,* **122,** 1385–1404.

Schiemann, R., M. G. Glazirina, and C. Schär, 2007: On the relationship between the Indian summer monsoon and river flow in the Aral Sea Basin. *Geophys. Res. Lett.,* **34,** L05706, doi:10.1029/2006GL028926.

——, D. Lüthi, and C. Schär, 2009: Seasonality and interannual variability of the westerly jet in the Tibetan Plateau region. *J. Climate,* **22,** 2940–2957.

Slingo, J., 2003: Monsoons: Overview. *Encyclopedia of Atmospheric Sciences,* J. Holton, J. Pyle, and J. Curry, Eds., Vol. 3, Elsevier, 1365–1370.

Smith, E. A., 1986: The structure of the Arabian heat low. Part II: Bulk tropospheric heat budget and implications. *Mon. Wea. Rev.,* **114,** 1084–1102.

Terao, T., 1998: Barotropic disturbances on intraseasonal time scales observed in the midlatitudes over the Eurasian continent during the northern summer. *J. Meteor. Soc. Japan,* **76,** 419–436.

Uppala, S. M., and Coauthors, 2005: The ERA-40 Re-Analysis. *Quart. J. Roy. Meteor. Soc.,* **131,** 2961–3012.

Wang, B., and LinHo, 2002: Rainy season of the Asian–Pacific summer monsoon. *J. Climate,* **15,** 386–398.

——, Q. Bao, B. Hoskins, G. Wu, and Y. Liu, 2008: Tibetan Plateau warming and precipitation changes in East Asia. *Geophys. Res. Lett.,* **35,** L14702, doi:10.1029/2008GL034330.

Yanai, M., C. Li, and Z. Song, 1992: Seasonal heating of the Tibetan Plateau and its effects on the evolution of the Asian summer monsoon. *J. Meteor. Soc. Japan,* **70,** 319–351.

Yasunari, T., 1986: Low-frequency interactions between the summer monsoon and the Northern Hemisphere westerlies. *J. Meteor. Soc. Japan,* **64,** 693–708.

Zhang, Z., J. C. L. Chan, and Y. Ding, 2004: Characteristics, evolution and mechanisms of the summer monsoon onset over Southeast Asia. *Int. J. Climatol.,* **24,** 1461–1482.